Electronic Supplementary Information for

Microhydrangeas with a high ratio of low valence MnO_X are capable of extremely fast degradation of organics

*Chengcheng Wang[1], Xin Wei[1], Yong Zhang[1], Jiali Fu[1], Hui Zhao[1] and Renjie Zhang[1,2,3]**

[1]Key Laboratory of Colloid and Interface Chemistry of the Ministry of Education of the P. R. China, Shandong University, Jinan 250100, P. R. China

[2]National Engineering Technology Research Center for Colloidal Materials, Shandong University, Jinan 250100, P. R. China

[3]Key Laboratory of Special Functional Aggregated Materials of the Ministry of Education of the P.R. China, Shandong University, Jinan 250100, P. R. China

EXPERIMENTAL

Materials

$MnSO_4 \cdot H_2O$, $(NH_4)_2SO_4$, $(NH_4)_2S_2O_8$, H_2O_2 (30 %), *p*-benzoquinone (*p*-BQ), *tert*-butanol (TBA), sulphanilic acid, acetic acid and $NaNO_2$ were purchased from Sinopharm Chemical Reagent Co., Ltd. 1-naphthylamine was purchased from Aladdin (Shanghai, China). Hydroxylamine hydrochloride ($NH_2OH \cdot HCl$) was purchased from Sigma-Aldrich. They were all analytical grade reagents and used without further

purification. Pure water with a resistivity of 18.2 MΩ·cm at 25 °C was used in all experiments.

Preparation of HRLV-MOMs

HRLV-MOMs were synthesized by a stirring hydrothermal method, where some composition are referred to literature.[1, 2] In brief, $MnSO_4 \cdot H_2O$ (0.18 g) and $(NH_4)_2SO_4$ (0.35 g) were dissolved in H_2O (30 mL) at room temperature to form a homogeneous solution. $(NH_4)_2S_2O_8$ (0.24 g) was dissolved in H_2O (10 mL) and dropped into the above solution under stirring. Then, the well mixed solution was transferred into a Teflon-lined autoclave (100 mL). The autoclave was maintained at 70 °C for 9 h in a silicon oil bath with a magnetic stirrer at 200 rpm. After reaction, the autoclave was cooled down to room temperature. The precipitates were collected by centrifugation (2000 rpm, 429 *g*, 3 min), washed with H_2O for 3 times and then dried at 40 °C in vacuum.

Catalysis performance of HRLV-MOMs for H_2O_2 to degrade MB

The catalytic performance of HRLV-MOMs was evaluated in the catalytic degradation of MB with H_2O_2. Firstly, MB (1.0 mL, 0.5 mg·mL^{-1}), HRLV-MOMs (1.0 mL, 1.0 mg·mL^{-1}) and H_2O (6.67 mL) were mixed and continuously stirred at room temperature. Then the catalytic reaction was started by addition of H_2O_2 (1.33 mL, 30 %), whose concentration (c_0 = 44.7 mg·mL^{-1}) is referred from the work with the largest reported efficiency by pure MnO_x catalyst.[3] Every a given time interval, 0.5 mL of the suspension was collected, then quickly diluted to 5 mL and immediately filtered with a syringe filter (0.22 μm). The concentration of the collected filtrate was measured at 664 nm by a UV-Vis spectrophotometer. To test the recyclability of HRLV-MOMs, the

recycled HRLV-MOMs were collected and washed with H_2O for 3 times for the next catalysis cycle. The degradation rate was calculated by $(A_0\text{-}A)/A_0$ based on the Lambert-Beer's law, where A_0 and A are the maximum absorbance of MB at 664 nm at the reaction time t = 0 and t, respectively.

Catalysis degradation mechanism of HRLV-MOMs

To distinguish the effect of different radicals, TBA or *p*-BQ was added as scavenger of ·OH or $O_2^{\cdot-}$ radicals, respectively. It is necessary to mention that the interference by the bright yellow *p*-BQ should be removed by deducting the absorbance of the mixture of *p*-BQ, HRLV-MOMs and H_2O_2 at the same concentration in the catalytic degradation experiments.

Quantitative calculation on ·OH radicals

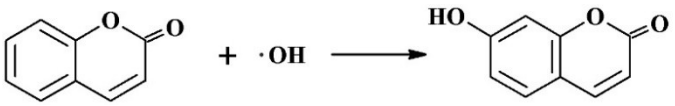

(S1)

·OH radicals interact with coumarin to generate 7-hydroxyl coumarin (eqn S1), whose fluorescence emission intensity is measured at 460 nm under the excitation wavelength of 332 nm. By recording fluorescence spectra of 7-hydroxyl coumarin generated from interaction of coumarin and ·OH radicals in the catalytic degradation system (Fig. S12b), the yield of ·OH radicals can be obtained indirectly according to the working curve of 7-hydroxyl coumarin (Fig. S12c) and the stoichiometric relationship between 7-hydroxyl coumarin and ·OH radicals.

Quantitative coumarin was mixed with the catalytic solution without MB to form 7-hydroxyl coumarin with ·OH radicals. 5 min later, 1.0 mL of the mixture was diluted

to 5.0 mL and filtered with a syringe filter (0.22 μm), whose fluorescence emission intensity was measured at 460 nm under the excitation wavelength of 332 nm. Fluorescence emission intensity of a series of 7-hydroxyl coumarin solutions in the concentration range of 1 to 25 mg·L^{-1} were measured to plot a linear working curve against concentration. The final mixture was diluted 5 times and according to the working curve (Fig. S12c), the equation is given by

$$c_{7-hydroxyl\ coumarin} = 0.02\, I_{460}\ (\mu g \cdot L^{-1}) \tag{S2}$$

where $c_{7\text{-}hydroxyl\ coumarin}$ is the mass concentration of 7-hydroxyl coumarin, I_{460} is the corresponding fluorescence emission intensity at 460 nm under the excitation wavelength of 332 nm.

The stoichiometric relationship between 7-hydroxyl coumarin and ·OH radicals based on eqn (S1) is 1: 1, so the yield in the weight ratio of ·OH radicals to HRLV-MOMs can be obtained as follows,

$$\begin{aligned} \omega_{\cdot OH} &= \frac{c_{7-hydroxyl\ coumarin}\ (mg \cdot L^{-1}) \cdot M_{\cdot OH}\ (g \cdot mol^{-1})}{M_{7-hydroxyl\ coumarin}\ (g \cdot mol^{-1}) \cdot c_{HRLV-MOMs}\ (mg \cdot mL^{-1})} \\ &= \frac{0.02\, I_{460} \cdot M_{\cdot OH}}{M_{7-hydroxyl\ coumarin} \cdot c_{HRLV-MOMs}}\ (mg \cdot g_{HRLV-MOMs}{}^{-1}) \end{aligned} \tag{S3}$$

All the catalytic reactions were carried out with HRLV-MOMs concentration ($c_{HRLV\text{-}MOMs}$) of 0.1 mg·mL^{-1}. $M_{\cdot OH}$ and $M_{7\text{-}hydroxyl\ coumarin}$ is the molar mass of ·OH radicals (17.0 g·mol^{-1}) and 7-hydroxyl coumarin (162.14 g·mol^{-1}), respectively. Thus,

$$\omega_{\cdot OH} = 0.021\, I_{460}\ (mg \cdot g_{HRLV-MOMs}{}^{-1}) \tag{S4}$$

The fluorescence emission intensity of 7-hydroxyl coumarin produced in the reaction of coumarin and ·OH radicals in the catalytic system was 3525 (Fig. S12b).

So, the yield of ·OH radicals in our catalytic mixture (10 mL) of HRLV-MOMs (0.1 $mg \cdot mL^{-1}$) and H_2O_2 ($c_0 = 44.7\ mg \cdot mL^{-1}$) at room temperature was 74.0 $mg \cdot g_{HRLV\text{-}MOMs}^{-1}$ according to eqn (S4).

Quantitative calculation on $O_2^{\cdot -}$ radicals

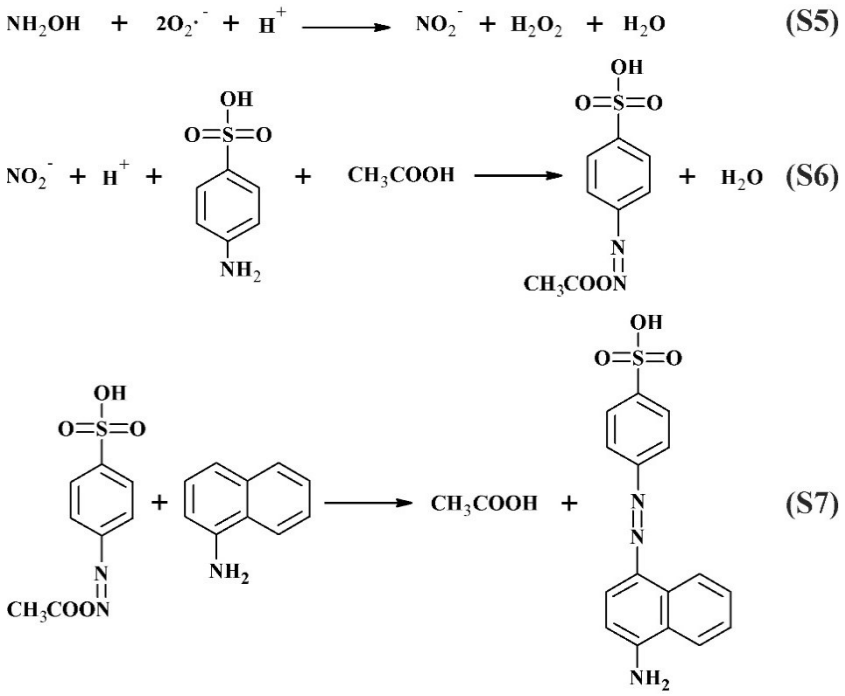

The amount of $O_2^{\cdot -}$ radicals was calculated based on a colorimetric method at the wavelength of 530 nm, which corresponds to the maximum absorbance of the finally formed azo dye complex.[4] Briefly, hydroxylamine (NH_2OH) reacts with $O_2^{\cdot -}$ radicals from the catalytic degradation system containing HRLV-MOMs, MB and H_2O_2 to produce NO_2^- (eqn S5). Then NO_2^- reacts with sulphanilic acid to form an azo compound (eqn S6), which interacts with 1-naphthylamine to generate an azo dye complex (eqn S7) with the intense absorbance at 530 nm. $NH_2OH \cdot HCl$ (0.21 g) was dissolved in H_2O (10 mL), then the NH_2OH solution (0.5 mL) was mixed with the catalytic solution without MB, followed by addition of a chromogenic solution (5.0 mL), the latter was obtained by mixing sulphanilic acid solution (0.4 %w/v), 1-

naphthylamine solution (0.1 %w/v) and acetic acid (25 %w/v). The mixture was stored in dark for 20 min to form reddish purple azo dye complex. A series of $NaNO_2$ solutions with concentration gradient were prepared and mixed with the chromogenic solution to form the azo dye complex solutions with concentration gradient. Then their absorbance at 530 nm was measured to plot a working curve of the azo dye complex against the concentration of NO_2^-. According to the working curve and stoichiometric relationship between the azo dye complex, NO_2^-, and $O_2^{\cdot -}$ radicals can be quantitatively calculated.

A series of $NaNO_2$ solutions with concentration gradient were prepared and mixed with the chromogenic solution to form the azo dye complex solutions with concentration gradient. Then their maximum absorbance at 530 nm was measured to plot a working curve of the azo dye complex against the concentration of NO_2^-. According to the working curve (Fig. S12e), the equation is given by

$$c_{azo\ dye\ complex} = 29.89\ A_{530}\ (\mu mol \cdot L^{-1}) \qquad \text{(S8)}$$

where $c_{azo\ dye\ complex}$ is molar concentration of the azo dye complex, A_{530} is the corresponding absorbance at 530 nm.

The stoichiometric relationship between different species based on eqn (S6) - (S7) in the main text is as follows,

$$c_{O_2^{\cdot -}} = 2\ c_{NO_2^-} = 2\ c_{azo\ dye\ complex} = 59.77\ A_{530}\ (\mu mol \cdot L^{-1}) \qquad \text{(S9)}$$

The yield in the weight ratio of $O_2^{\cdot -}$ radicals to HRLV-MOMs can be calculated by

$$\omega_{O_2^{\cdot -}} = \frac{c_{O_2^{\cdot -}}\ (\mu mol \cdot L^{-1}) \cdot M_{O_2^{\cdot -}}\ (g \cdot mol^{-1})}{c_{RHRLV-MOMs}\ (mg \cdot mL^{-1})} \qquad \text{(S10)}$$

All the catalytic reactions were carried out with HRLV-MOMs concentration (c_{HRLV-}

$_{MOMs}$) of 0.1 mg·mL^{-1} and $M_{O_2^{\cdot-}}$ is the molar mass of $O_2^{\cdot-}$ radicals, 32.0 g·mol^{-1}. Thus,

$$\omega_{O_2^{\cdot-}} = 19.13\ A_{530}\ (mg \cdot g_{HRLV-MOMs}{}^{-1}) \quad \text{(S11)}$$

The absorbance of the azo dye complex from NO_2^- produced in the reaction of NH_2OH and $O_2^{\cdot-}$ radicals in the catalytic system was 0.348 (Fig. S12f). So, the yield of $O_2^{\cdot-}$ radicals in our catalytic mixture (10 mL) of HRLV-MOMs (0.1 mg·mL^{-1}) and H_2O_2 (c_0 = 44.7 mg·mL^{-1}) at room temperature was 6.6 mg·$g_{HRLV\text{-}MOMs}{}^{-1}$ according to eqn S11.

Characterization

Field emission scanning electron microscopy (SEM) and elemental mapping were performed on a SU8010 (Hitachi, Japan) instrument (an accelerating voltage, 5 kV). Transmission electron microscopy (TEM) images of HRLV-MOMs were obtained with a JEM-1011 (Jeol, Japan) under an accelerating voltage of 100 kV. High resolution TEM (HRTEM) images and selected area electron diffraction (SAED) of HRLV-MOMs were obtained on a JEOL-2100F TEM (Jeol, Japan) with an acceleration voltage of 200 kV. X-ray diffraction (XRD) measurement of HRLV-MOMs was obtained by a D8 Advance X-ray diffractometer (Bruker, Germany) at 40 kV and 40 mA (Cu (Kα) radiation, λ = 1.54184 Å). X-ray photoelectron spectroscopy (XPS) was performed on a Phi 5300 ESCA (Perkin Elmer, USA) with the Mg (Kα) irradiation (X-ray energy, 1253.6 eV, spot area, 1.0×3.5 mm^2). Fourier transform infrared (FTIR) spectra of HRLV-MOMs were recorded with a Vertex-70 FTIR spectrometer (Bruker, Germany), where they were mixed with KBr and pressed into a thin platelet. Thermogravimetric analysis (TGA) of HRLV-MOMs was carried out from 25 to 800 ºC in N_2 at a heating

rate of 10 ºC·min^{-1} with a TGA-50 thermal analyzer (SHIMADZU, Japan). Powder nitrogen (N_2) adsorption-desorption isotherms were recorded with an ASAP 2020 HD88 instrument (Micromeritics, USA). Ultraviolet-visible (UV-Vis) absorption spectra were measured with a double-beam spectrophotometer (UV-2550, Shimadzu Co., Japan). Fluorescence emission spectra were recorded with a fluorescence spectrophotometer (F-7000, HITACHI, Japan). Zeta potential of dilute HRLV-MOMs suspension was measured by a Zetasizer Nano-ZS90 (Malvern Instruments Ltd., UK) at room temperature.

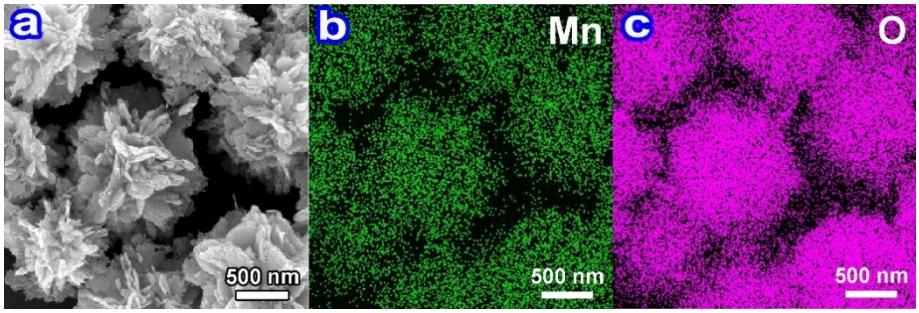

Fig. S1 (a) SEM images of monodisperse HRLV-MOMs and corresponding elemental mapping images of the (b) Mn and (c) O element.

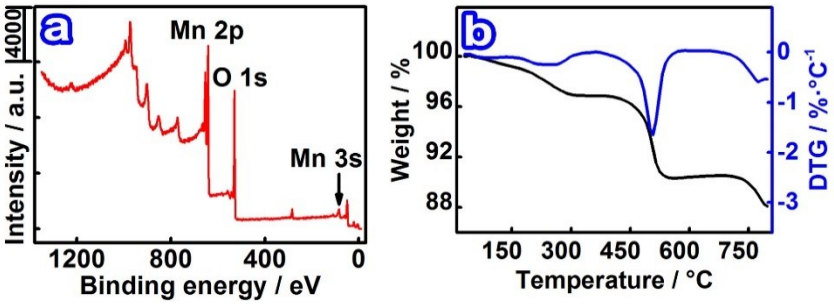

Fig. S2 (a) XPS survey spectrum, (b) TGA curves of HRLV-MOMs.

The weight loss of about 1.0 wt% is due to the adsorbed water on the surface of HRLV-MOMs below 160 °C while the weight loss of 2.2 wt% from 160 to 350 °C is

ascribed to the desorption of the crystal water existing in nanosheets of HRLV-MOMs. The weight loss between 380 and 600 °C is due to the reduction of MnO_2 to Mn_2O_3 accompanied by evolution of oxygen. The weight loss between 700 and 800 °C corresponds to the transformation from Mn_2O_3 to Mn_3O_4 accompanied by oxygen release[5] as Mn_3O_4 is in stable state at high temperature.

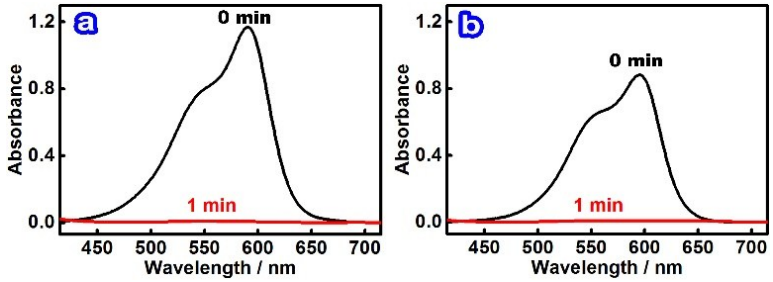

Fig. S3 Visible absorption spectra of (a) crystal violet (c_0 = 0.05 mg·mL^{-1}) with the maximum absorbance at 590 nm and (b) ethyl violet (c_0 = 0.05 mg·mL^{-1}) with the maximum absorbance at 596 nm over time in the presence of HRLV-MOMs (0.1 mg·mL^{-1}) and H_2O_2 (c_0 = 44.7 mg·mL^{-1}).

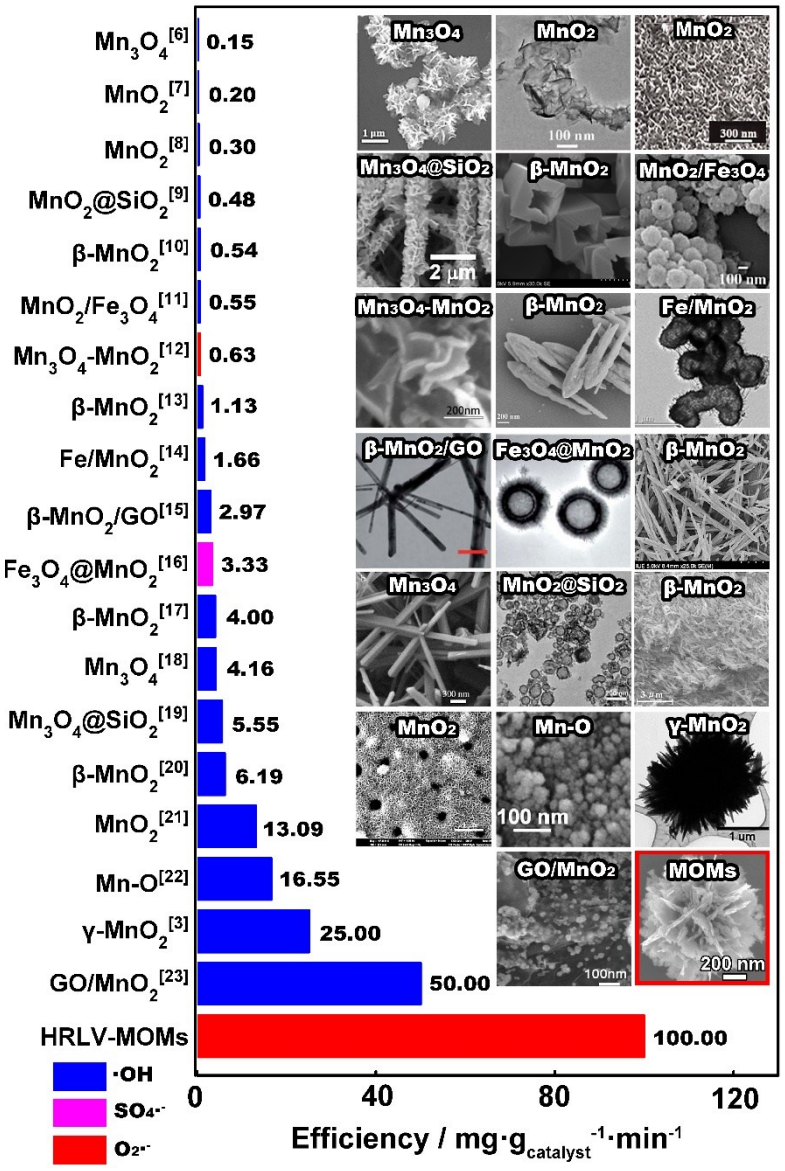

Fig. S4 Catalytic degradation efficiency comparison of different morphologies of MnO_x for MB degradation by the main radicals ·OH or the radicals $SO_4^{\cdot -}$ and $O_2^{\cdot -}$. The insets are adapted from references with copyright from Elsevier, Wiley-VCH, American Chemical Society and The Royal Society of Chemistry, respectively.

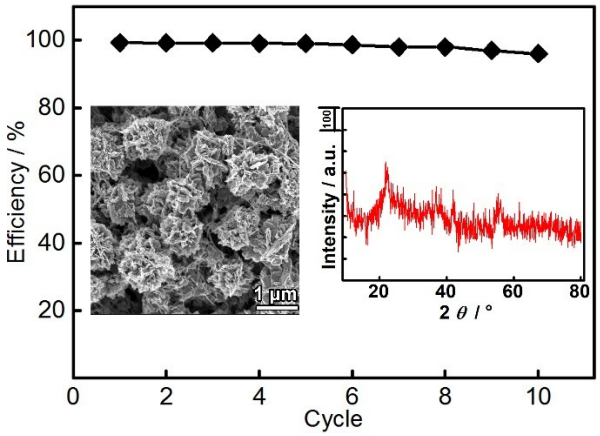

Fig. S5 The recyclability of the HRLV-MOMs (0.1 mg·mL^{-1}) using successive catalytic degradation of MB (c_0 = 0.05 mg·mL^{-1}) with H_2O_2 (c_0 = 44.7 mg·mL^{-1}). The insets are the SEM image and XRD pattern of the HRLV-MOMs after 10 cycles of catalysis.

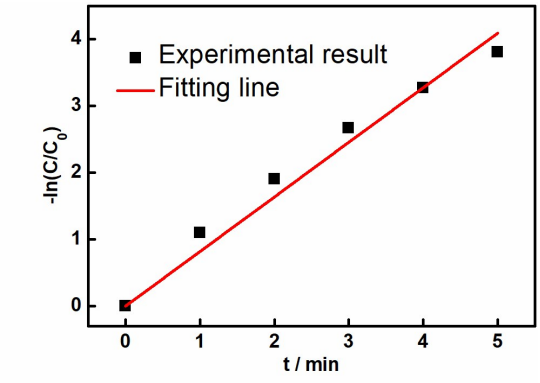

Fig. S6 Linear fitting of experimental data by first-order kinetic model.

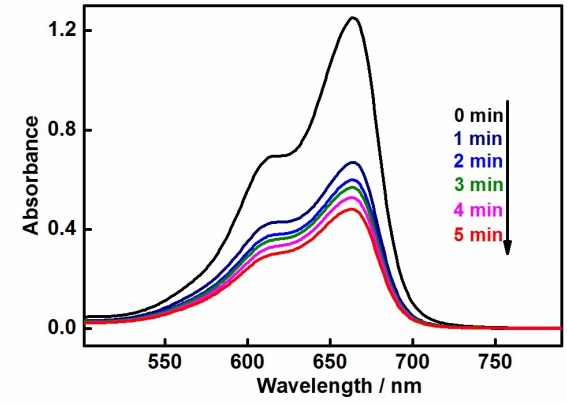

Fig. S7 Visible absorption spectra of MB (c_0 = 0.05 mg·mL^{-1}) over time in the presence of HRLV-MOMs (0.1 mg·mL^{-1}) and H_2O_2 (c_0 = 44.7 mg·mL^{-1}) in N_2-saturated

solution.

When the catalytic degradation experiment is carried out in N_2-saturated solution (Fig. 3c in the main text and Fig. S7), the efficiency decreases remarkably, which indicates that dissolved O_2 also contributes to high catalytic performances. Dissolved O_2 can interact with the electrons (e^-) in negatively charged HRLV-MOMs with Zeta potential of -17.6 mV to generate $O_2^{\cdot-}$ radicals,[12] which contribute to MB degradation.

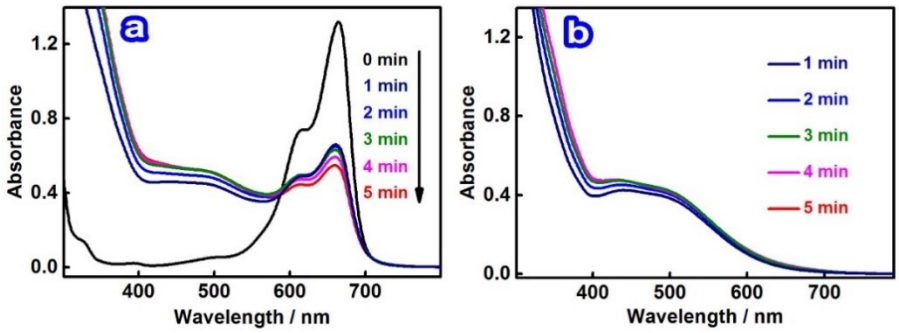

Fig. S8 (a) UV-Vis absorption spectra of MB (c_0 = 0.05 mg·mL^{-1}) over time with interference of *p*-BQ (5.4 mg·mL^{-1}) containing HRLV-MOMs (0.1 mg·mL^{-1}) and H_2O_2 (c_0 = 44.7 mg·mL^{-1}). (b) UV-Vis absorption spectra of the mixture of HRLV-MOMs (0.1 mg·mL^{-1}), H_2O_2 (c_0 = 44.7 mg·mL^{-1}) and *p*-BQ (c_0 = 5.4 mg·mL^{-1}).

The interfering peaks (Fig. S8a) of added bright yellow *p*-BQ can be deducted from the catalytic spectraby deducing the spectra of *p*-BQ, H_2O_2 and HRLV-MOMs with the same concentration of catalytic experiments (Fig. S8b). The final spectra are shown in Fig. S11.

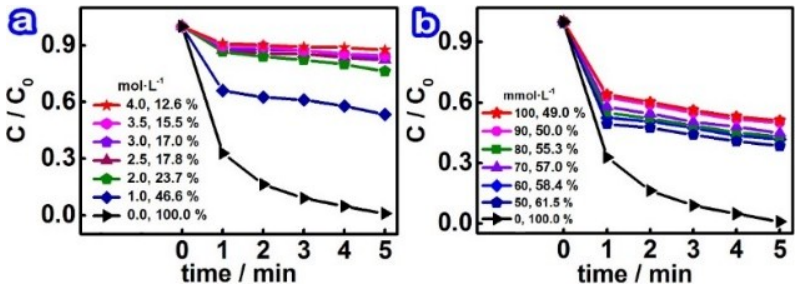

Fig. S9 The catalytic degradation efficiency against time with different addition of (a) TBA and (b) *p*-BQ with MB (c_0 = 0.05 mg·mL^{-1}), HRLV-MOMs (0.1 mg·mL^{-1}) and H_2O_2 (c_0 = 44.7 mg·mL^{-1}). The corresponding visible absorption spectra are shown in Fig. S10 and S11.

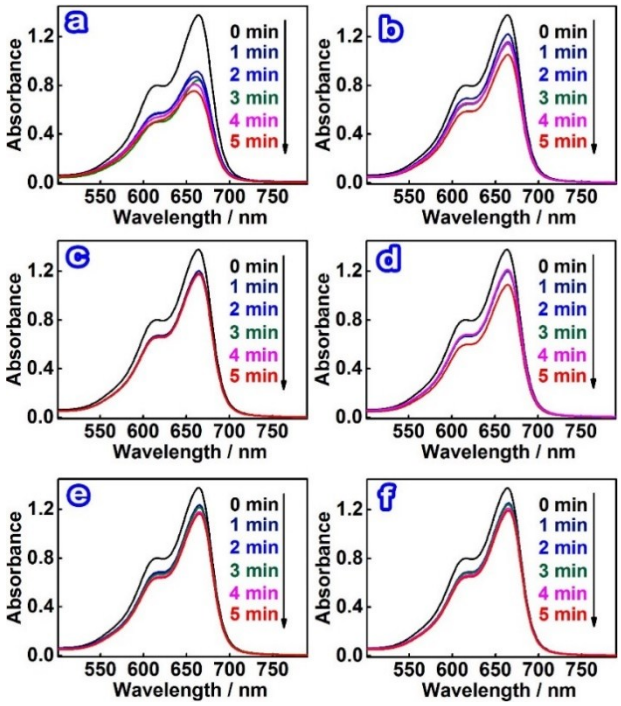

Fig. S10 Visible absorption spectra of MB (c_0 = 0.05 mg·mL^{-1}) over time with different concentration of TBA in the mixture containing HRLV-MOMs (0.1 mg·mL^{-1}) and H_2O_2 (c_0 = 44.7 mg·mL^{-1}). (a) 1.0, (b) 2.0, (c) 2.5, (d) 3.0, (e) 3.5 and (f) 4.0 mol·L^{-1}.

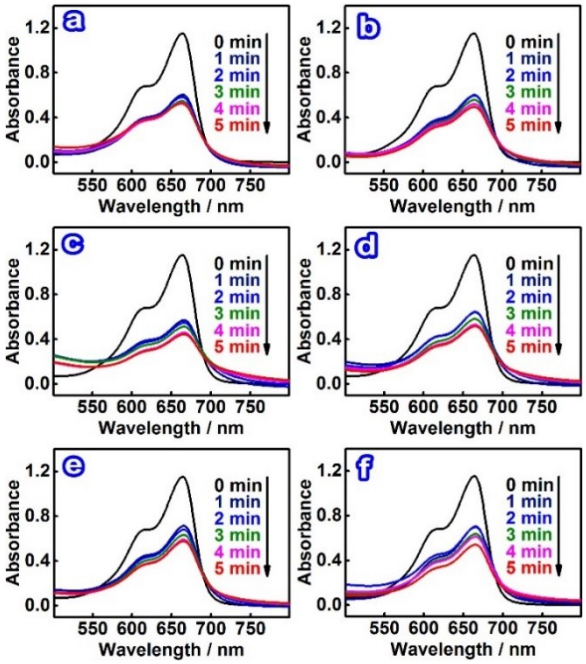

Fig. S11 Visible absorption spectra of MB (c_0 = 0.05 mg·mL^{-1}) over time with different concentration of *p*-BQ in the mixture containing HRLV-MOMs (0.1 mg·mL^{-1}) and H_2O_2 (c_0 = 44.7 mg·mL^{-1}). (a) 50, (b) 60, (c) 70, (d) 80, (e) 90 and (f) 100 mmol·L^{-1}.

By increasing the concentration of the scavengers, the optimal addition of TBA and *p*-BQ are obtained. The c/c_0 becomes the maximum when TBA increases to 4.0 mol·L^{-1} (Fig. S9a and S10) and p-BQ increases to 100 mmol·L^{-1} (Fig. S9b and S11).

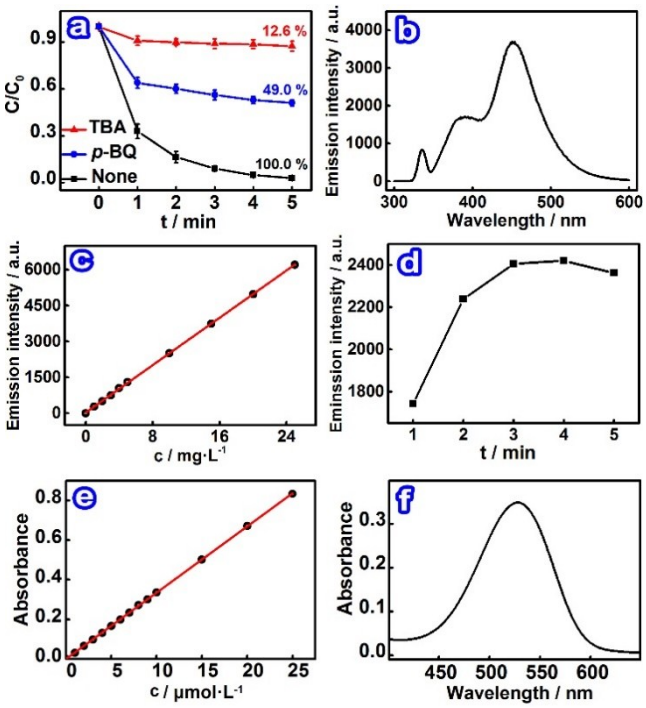

Fig. S12 (a) Catalytic degradation of MB with or without scavengers (TBA for ·OH radicals and *p*-BQ for $O_2^{\cdot-}$ radicals). (b) The fluorescence emission intensity of 7-hydroxyl coumarin produced in the reactions of coumarin and ·OH radicals in the catalytic degradation system, (c) the working curve of the fluorescence emission intensity of 7-hydroxyl coumarin against its concentration for quantitatively measurement of ·OH radicals. (d) The fluorescence emission intensity of 7-hydroxyl coumarin produced from the reaction of coumarin (0.3 mg·mL^{-1}) and ·OH radicals at different time in the catalytic degradation system. (e) The linear working curve of the absorbance of the azo dye complex against the concentration of NO_2^- for quantitatively measurement of $O_2^{\cdot-}$ radicals. (f) Visible absorption spectra of an azo dye complex relating to NO_2^- produced in the reactions of NH_2OH and $O_2^{\cdot-}$ radicals in the catalytic degradation system containing HRLV-MOMs (0.1 mg·mL^{-1}) and H_2O_2 (c_0 = 44.7 mg·mL^{-1}). The corresponding fluorescence spectra of (a), (c), (d) and (e) are shown in Fig. S10f, S11f, S13c, S13d and S14, respectively.

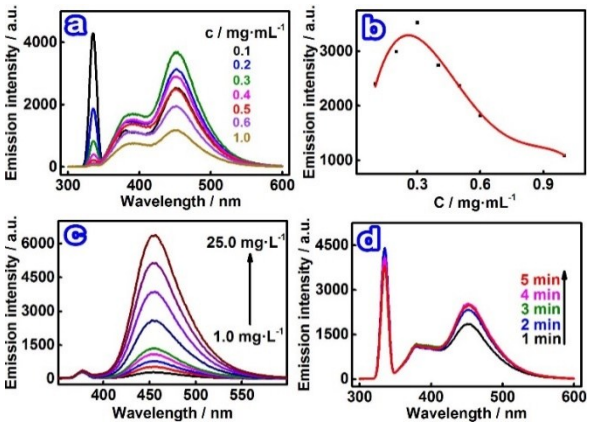

Fig. S13 Fluorescence spectra of 7-hydroxyl coumarin (a) produced from the reaction of ·OH radicals with different concentration of coumarin in the concentration range of 0.1 to 1.0 mg·mL^{-1} corresponding to (b) fitting curve of fluorescence emission intensity at 460 nm against the concentration of coumarin in catalytic degradation process. (c) Fluorescence spectra of 7-hydroxyl coumarin with concentration gradient and (d) against time during catalytic degradation process. The catalytic degradation system contains HRLV-MOMs (0.1 mg·mL^{-1}) and H_2O_2 (c_0 = 44.7 mg·mL^{-1}).

The concentration of added coumarin in the catalytic degradation system is optimized (Fig. S13a) because inadequate coumarin is not enough to interact with ·OH radicals generated from the catalytic degradation system while excess coumarin would lead to fluorescence quenching.[24] When 0.3 mg·mL^{-1} of coumarin is added to the catalytic degradation system, the fluorescence emission is the most intense (Fig. S13b).

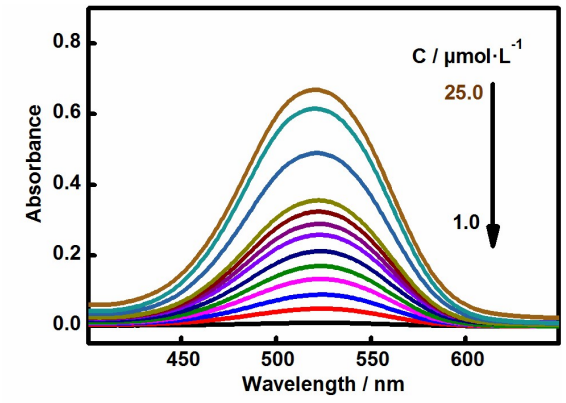

Fig. S14 Visible absorption spectra of the azo dye complex against concentrations in the catalytic degradation system containing HRLV-MOMs (0.1 mg·mL^{-1}) and H_2O_2 (c_0 = 44.7 mg·mL^{-1}) for quantitative measurement of $O_2^{\cdot -}$ radicals.

References

1. X. Wang and Y. Li, *Chem.-Eur. J.*, 2003, **9**, 300-306.
2. X. Wang and Y. Li, *J. Am. Chem. Soc.*, 2002, **124**, 2880-2881.
3. E. J. Kim, D. Oh, C. S. Lee, J. Gong, J. Kim and Y. S. Chang, *Catal. Today*, 2017, **282**, 71-76.
4. S. H. Do, B. Batchelor, H. K. Lee and S. H. Kong, *Chemosphere*, 2009, **75**, 8-12.
5. J. Wang, G. Zhang, L. Ren, L. Kang, Z. Hao, Z. Lei and Z. H. Liu, *Cryst. Growth Des.*, 2014, **14**, 5626-5633.
6. Y. L. Wang, L. Zhu, X. Yang, E. L. Shao, X. Y. Deng, N. Liu and M. H. Wu, *J. Mater. Chem. A*, 2015, **3**, 2934-2941.
7. G. Zhao, J. Li, X. Ren, J. Hu, W. Hu and X. Wang, *RSC Adv.*, 2013, **3**, 12909-12914.
8. Y. X. Zhang, X. L. Guo, M. Huang, X. D. Hao, Y. Yuan and C. Hua, *J. Phys.*

Chem. Solids, 2015, **83**, 40-46.

9. X. Wang, L. Dou, L. Yang, J. Yu and B. Ding, *J. Hazard. Mater.*, 2017, **324**, 203-212.

10. X. Zheng, T. Lin, G. Cheng, B. Lan, M. Sun and L. Yu, *Adv. Powder Technol.*, 2015, **26**, 622-625.

11. L. Zhang, J. Lian, L. Wu, Z. Duan, J. Jiang and L. Zhao, *Langmuir*, 2014, **30**, 7006-7013.

12. J. H. Zhao, J. Nan, Z. W. Zhao, N. Li, J. Liu and F. Y. Cui, *Appl. Catal., B*, 2017, **202**, 509-517.

13. G. Cheng, L. Yu, T. Lin, R. Yang, M. Sun, B. Lan, L. Yang and F. Deng, *J. Solid State Chem.*, 2014, **217**, 57-63.

14. R. Huang, Y. Liu, Z. Chen, D. Pan, Z. Li, M. Wu, C. H. Shek, C. M. L. Wu and J. K. L. Lai, *ACS Appl. Mater. Inter.*, 2015, **7**, 3949-3959.

15. J. Mei and L. Zhang, *RSC Adv.*, 2015, **5**, 14843-14850.

16. S. W. Zhang, Q. H. Fan, H. H. Gao, Y. S. Huang, X. Liu, J. X. Li, X. J. Xu and X. K. Wang, *J. Mater. Chem. A*, 2016, **4**, 1414-1422.

17. H. J. Cui, H. Z. Huang, M. L. Fu, B. L. Yuan and W. Pearl, *Catal. Commun.*, 2011, **12**, 1339-1343.

18. Z. Bai, B. Sun, N. Fan, Z. Ju, M. Li, L. Xu and Y. Qian, *Chem.-Eur. J.*, 2012, **18**, 5319-5324.

19. Q. Meng, S. Xiang, W. Cheng, Q. Chen, P. Xue, K. Zhang, H. Sun and B. Yang, *J. Colloid Inter. Sci.*, 2013, **405**, 28-34.

20. C. L. Yu, G. Li, L. F. Wei, Q. Z. Fan, Q. Shu and J. C. Yu, *Catal. Today*, 2014, **224**, 154-162.

21. Y. X. Zhang, X. D. Hao, F. Li, Z. P. Diao, Z. Y. Guo and J. Li, *Ind. Eng. Chem. Res.*, 2014, **53**, 6966-6977.

22. B. Debnath, A. S. Roy, S. Kapri and S. Bhattacharyya, *Chemistryselect*, 2016, **1**, 4265-4273.

23. J. Y. Qu, L. Shi, C. X. He, F. Gao, B. B. Li, Q. Zhou, H. Hu, G. H. Shao, X. Z. Wang and J. S. Qiu, *Carbon*, 2014, **66**, 485-492.

24. K. I. Ishibashi, A. Fujishima, T. Watanabe and K. Hashimoto, *Electrochem. Commun.*, 2000, **2**, 207-210.